

**NUCLEAR ENERGY RESEARCH INITIATIVE (NERI)
ANNUAL PROGRESS REPORT**

Project Title:

Incorporation of Integral Fuel Burnable Absorbers Boron and Gadolinium into Zirconium-Alloy Fuel Clad Material

Award No.: DE-FG07-02SF22617

Project No.: 2002-044

Final Report

Covering Period: September 2002 to September 2003

DoE Contact: Dr. Kenny Osborne (INEEL)

Lead Organization and Address:

University of Wisconsin, Madison
Department of Engineering Physics
1500 Engineering Drive
Madison, WI 53706
PI: Dr. Kumar Sridharan, Senior Scientist
Tel. No.: (608) 263-4789
kumar@engr.wisc.edu
Co-PI: Dr. Michael Corradini, Professor

Collaborating Organizations:

Sandia National Laboratories, Albuquerque, NM
Co-PI: Dr. Timothy Renk, Member of Technical Staff

Westinghouse Electric Company – Science and Technology Department,
Pittsburgh, PA

Co-PI: Dr. Edward Lahoda, Consulting Engineer

**PROTECTED DATA: PAGES 36 TO 64
PATENTABLE DATA: PAGES 65 TO 68**

Submitted on:

December 13, 2004

“The material is based upon work supported by the U.S. Department of Energy under the Award No. DE-FG07-02SF22617. Any opinions, findings, and conclusions or recommendations are those of the authors and do not necessarily reflect the views of the Department of Energy”

EXECUTIVE SUMMARY

Long-lived fuels require the use of higher enrichments of ^{235}U or other fissile materials. Such high levels of fissile material lead to excessive fuel activity at the beginning of life. To counteract this initial reactivity, integral fuel burnable absorbers (IFBA) are added to some rods in the fuel assembly. The two commonly used IFBA elements are gadolinium, which is added as gadolinium-oxide to the UO_2 powder, and boron, which is applied as a zirconium-diboride coating on the UO_2 pellets using plasma spraying or chemical vapor deposition techniques. The incorporation of IFBA into the fuel has to be performed in a nuclear-regulated facility that is physically separated from the main plant. These operations tend to be very costly because of their small volume and can add from 20 to 30% to the manufacturing cost of the fuel. Other manufacturing issues that impact cost and performance are maintaining the correct levels of dosing, the reduction in fuel melting point due to IFBA additions, parasitic neutron absorption at fuel's end-of-life, and build-up of pressure due to the formation of transmutation gases.

The goal of the proposed research was to develop an alternative approach that involves incorporation of boron or gadolinium into the outer surface of the fuel cladding material rather than as an additive to the fuel pellets. This paradigm shift will allow for the introduction of the IFBA in a non-nuclear regulated environment and will obviate the necessity of additional handling and processing of the fuel pellets. This could represent significant cost savings and potentially lead to greater reproducibility and control of the burnable fuel in the early stages of the reactor operation.

The surface alloying for this research was performed using the IBEST (Ion Beam Surface Treatment) process at Sandia National Laboratories, the developer of this process in the United States. IBEST involves the delivery of intense, energetic ion beam pulses onto the surface of a material, near-surface melting, and rapid solidification. The non-equilibrium nature of such processing allows for surface alloying in excess of the thermodynamically dictated solubility limits, an effect that is particularly relevant to this research due to the negligible solubility of boron and gadolinium in zirconium. University of Wisconsin performed the near surface materials characterization and aided Sandia in process optimization, coordinated the overall program, and promoted educational activities. Westinghouse performed the steam/water autoclave tests on the surface-treated samples and conducted a detailed process manufacturability evaluation.

Two zirconium alloys Zirlo and Zircaloy-4 were sputter deposited with gadolinium and boron and subjected to the IBEST process. The energetic ion species used for gadolinium was neon and for boron it was nitrogen. Optimization work showed that complete alloying of gadolinium was achieved in the ion energy range of 1-2 kJ/cm^2 , whereas for boron complete alloying was achieved in the ion energy range of 4-5 kJ/cm^2 . This was supported by a number of numerical simulations and characterized by using a suite of materials characterization techniques. Autoclave testing at 800F in a steam environment showed that the gadolinium alloyed samples exhibited unacceptable levels of oxidation. The boron alloyed samples showed remarkable resistance to corrosion and were comparable to the untreated zirconium alloys. Boron thus emerged as a superior candidate for such an alloying treatment. Detailed cost analysis performed by Westinghouse based on operations at their commercial plants showed that with such surface modification, the cost per cladding tube would be about \$33 compared to the \$11 present cost for an untreated cladding tube. Upon approval from the NERI committee, initial investigation of an alternative Westinghouse technology based on cold-spray powder spray process was performed. It was noted that cold-spraying of ZrB_2 powders to form a coating on the surface of the cladding materials holds considerable promise from the standpoint of costs, corrosion resistance, and IFBA incorporation.

PROJECT BACKGROUND: The surface alloying of boron and gadolinium into zirconium cladding tube rather than their incorporation in fuel pellets can lead to significant economic savings and will allow for the use of higher enrichment fuels in the current and future nuclear reactor systems. However, the alloying of boron and gadolinium into the zirconium alloy bulk (rather than the surface) would be undesirable because of their deleterious effect on neutron transparency and bulk properties, and from the standpoint of stresses generated in the walls of the cladding due to the formation of gaseous products such as helium. Alloying of these elements to the outer surface of the cladding overcomes these problems. The thickness and stability of the alloyed layer should be such that it provides adequate neutron absorption in the initial reactivity stage, without too quickly dissolving or corroding into the adjacent steam/water environment.

This project was performed collaboratively between three participating institutions, a University, a National Laboratory, and an Industry. University of Wisconsin-Madison was the lead organization and was responsible for materials preparation and characterization before and after surface treatments, and for post-autoclave testing materials analysis. University of Wisconsin was also responsible for the overall coordination of the research program and educational aspects of the project. Sandia National Laboratories, Albuquerque was responsible for the ion-based surface treatment of the alloys and theoretical modelling of the surface alloying process. Westinghouse Science and Technology, Pittsburgh was responsible for autoclave testing of the surface treated samples and manufacturability evaluation of the process.

EXPERIMENTAL METHODOLOGY AND PROCEDURES

A. Initial Issues and Proposed Resolutions:

Immediately upon its inception in September 2002, the project's focus was on identification and resolution of a number of scientific and technical issues brought forth by the three collaborating groups. These included detailed discussions on issues such as sample size and thickness, surface roughness, IFBA sputter layer thickness, the types of energetic ion to be used for the ion-based surface treatment, and scheduling. Some of these issues and their proposed solutions are elaborated below:

(i) Substrate material procurement: Two zirconium alloys used widely in the nuclear industry for fuel cladding, Zirlo and Zircaloy-4, were used as substrate materials for this

research. It was decided that throughout the term of this project a single vendor should supply these materials, and preferably from a single processing batch, in order to avoid even minor compositional and structural variations in the substrate. It was decided that Westinghouse would supply the substrate material required for the entire project.

(ii) Substrate sample size: From the standpoint of autoclave testing at Westinghouse, samples with larger exposure area-to-weight ratio were considered desirable in order to enhance the resolution in weight change measurements. However, from the standpoint of IBEST processing at Sandia National Laboratories, 0.75"x0.75" sample size was deemed ideal which would allow for eight such samples to be treated in one batch at Sandia's IBEST facility. It was decided that a sample size of 0.75"x0.75" and a thickness of 0.02" would be used. The thickness was based on the accuracy in weight change measurements as well as the currently used fuel cladding thickness.

(iii) Substrate surface: The zirconium alloy strips provided by Westinghouse were not pickled (process of removing surface oxides). It was initially suggested that the surface roughness of samples be identical to that of the fuel cladding tube. However, from the standpoint of characterization and basic materials science, a well-polished surface was deemed desirable. It was decided that the University of Wisconsin would undertake the task of pickling the zirconium alloy sheets, cutting them to the required sample size, and polishing the samples. For initial process optimization work, only one side was polished and treated by the IBEST process at Sandia. For those samples intended for autoclave testing, both sides would be polished and surface treated. For these two-side treated samples, a hole (about 1/16th dia.) was drilled at the center of one of the edges for convenient suspension in the specimen rack of the autoclaves at Westinghouse.

(iv) Sputtering: It was decided that sputtering would be performed at Sandia National Laboratories because of specialized personnel expertise available at Sandia, and also because of their prior experience in the specific area gadolinium and boron sputtering.

(v) IFBA material to be sputtered: Boron and gadolinium were the two IFBA materials that were proposed for research in the present study. It was decided that initial experiments would be performed with gadolinium, based on the reasoning that it has a lower heat of fusion than boron and consequently it is more amenable to sputtering and IBEST processing. Also, gadolinium sputter targets are substantially cheaper than boron, and it appeared logical that initial trouble-shooting be done with a cheaper material.

(vi) Thickness of the sputtered IFBA layer: Based on preliminary calculations, the amount of IFBA material required for neutron absorption, as well as theoretical simulations of melt zone thickness in IBEST, it was decided to initiate the research with an IFBA sputter film thickness in the range of about 0.5 μm to 1.5 μm . Figure 1 shows the conversion between weight percent Gd in the fuel and the equivalent thickness of the Gd film using typical cladding geometries and weight-volume conversions for Gd.

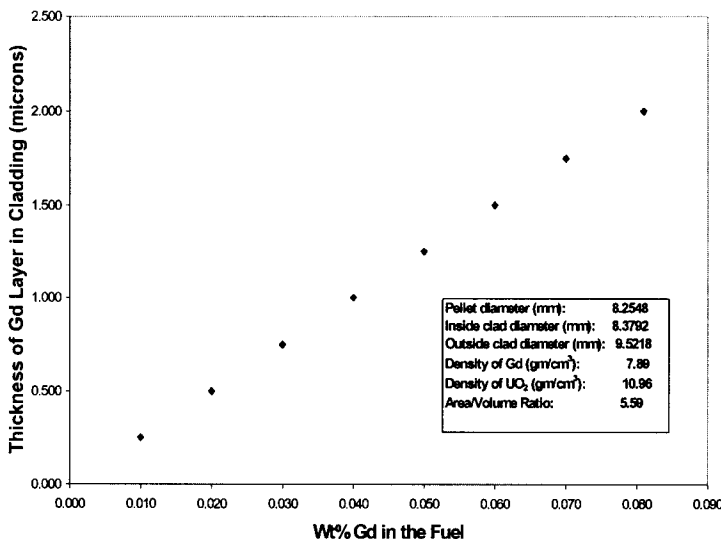


Figure 1. Plot showing the thickness of Gd film in the outer regions of the cladding tube as a function of the weight percent Gd in the uranium-dioxide fuel.

(vi) Ion species for the IBEST process: Ion species such as N, O, or C are used for IBEST processing. Work on Gd was performed using neon ions however for boron which has a much higher heat of melting than Gd, nitrogen ions were used because they impart a much higher energy on the materials surface compared to neon. In this case no nitride was observed to form in the surface layer.

B. Zirconium Alloys Procurement and Sample Preparation

Strips of Zirlo and Zircaloy-4 (12" length, 2" width, and 0.02" thickness, Figure 2) alloys were supplied by Westinghouse Corporation to the University of Wisconsin, where they were pickled in a (50% nitric acid + 5% hydrofluoric acid + 45% water) mixture solution bath, at room temperature for 15 minutes. This pickling step was deemed essential because the surface treatment(s) central to the proposed research affect a few

microns of the subsurface region and the presence of any oxides would interfere with this process and subsequent characterization work.

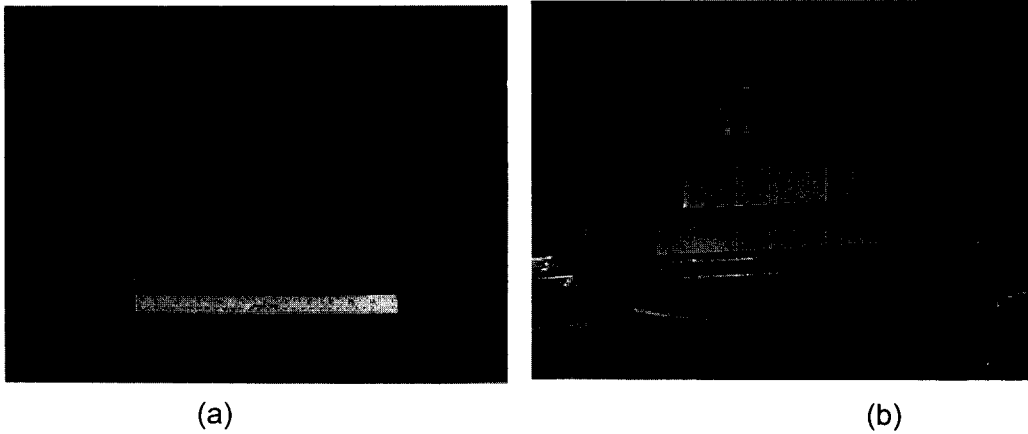


Figure 2. (a) Photograph of the zirconium alloy strips (0.02" thickness) provided for this study by Westinghouse, and (b) the strips being 'pickled' in an acid bath mixture at the University of Wisconsin.

The pickled strips of each alloy were then sheared into samples of 0.75"x0.75", and metallographically polished by grinding initially with a 600 and 800 grit silicon-carbide paper followed by polishing using 1 μ m diamond paste suspended in an oil emulsion. This level of surface finish is necessary to accurately characterize the micro/nanostructural developments in the near-surface regions as a result of the sputtering and IBEST treatment. Figure 3 shows the samples used in this research.

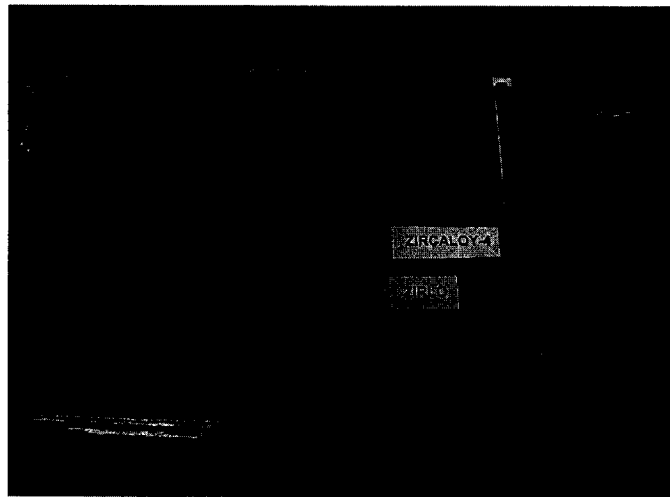


Figure 3. Photograph of sample test flats cut to 0.75" x 0.75" size (left) and after metallographic polishing (right).

C. STUDIES OF GADOLINIUM SURFACE ALLOYING

Simulation codes to gain predictive capability of process:

To gain a predictive capability of the outcome of our sputter deposition and IBEST experiments and for the selection of appropriate experimental parameters, computer simulations, TRIM (Transport Induced Mixing) an ion-materials interaction code and a 1-D numerical code to predict surface melting and re-solidification were performed. The TRIM code calculates the concentration profile and penetration depth of ions in a substrate as a function of depth. The 1-D numerical code uses the materials' thermal properties as input parameters and calculates, temperature profiles with time at various depths below the surface of the material, melt and solidification wave velocities, and melt depth with time. Figures 4 shows the application of these codes for predicting melt depth.

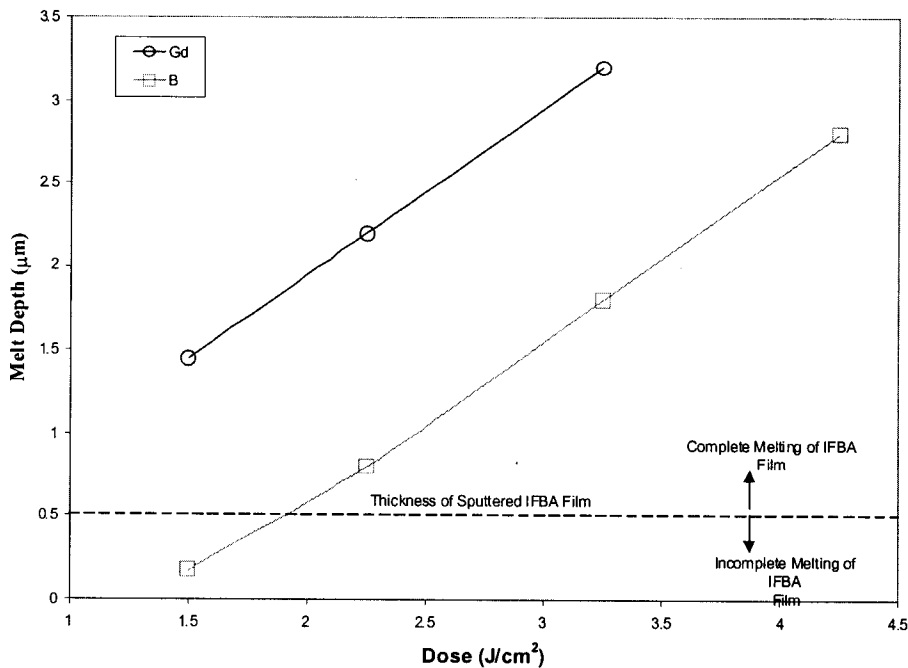


Figure 4. Computer simulations for predicting melt depth as a function of ion-dose for 0.5 μ m gadolinium and boron sputtered films. Note that at doses below about 1.8 J/cm² the 0.5 μ m boron film has not completely melted throughout its thickness.

Another example of the use of such simulations is shown in Figure 5, which has been performed for Gd film on Zr and bombarded with neon ions using beam energy of 2.4 J/cm^2 and for beam pulse ranging from 0 to 450ns. The code indicates that Gd layer fully melts after which the Zr melts to depths of $1.5\mu\text{m}$. Zr melt duration is about $1.3\mu\text{s}$ and Gd melt duration is $3\mu\text{s}$.

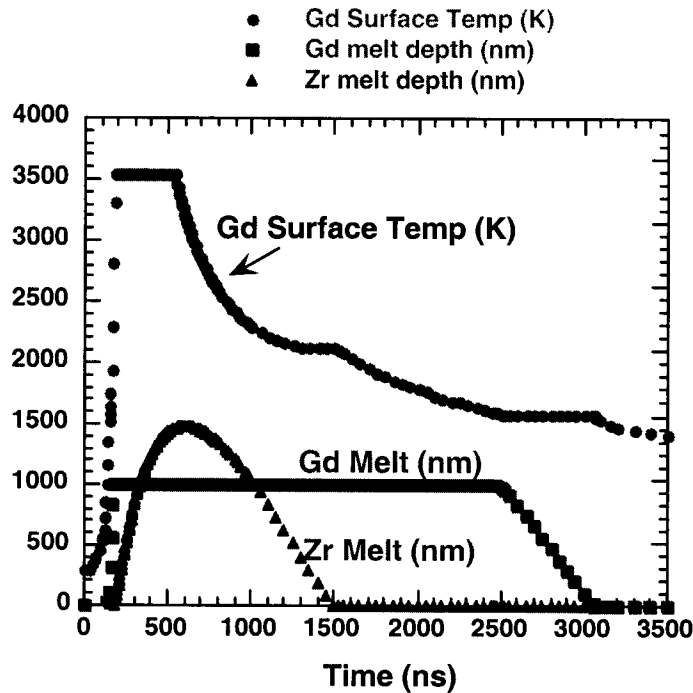
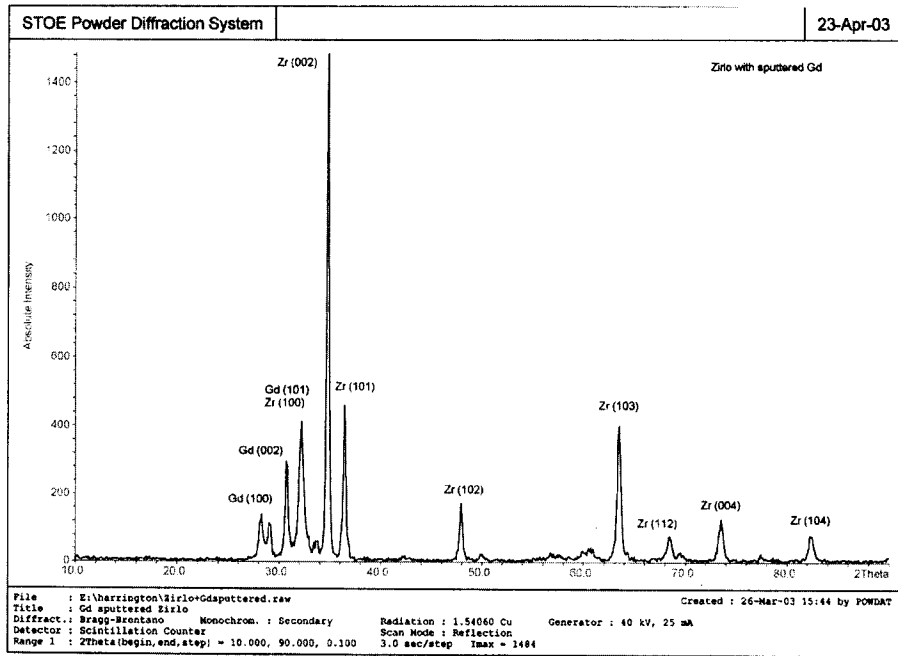


Figure 5. An example of 1-D simulation code that is being used to determine the required Gd layer thickness and process parameters.

Gadolinium sputter deposition:

Initially a $0.5\mu\text{m}$ thick Gd film was sputter deposited on the samples using a Gd sputter cathode procured specifically for this study. Figure 6 show the x-ray diffraction pattern for a Gd sputtered Zirlo sample substrate.



(a)

Figure 6. X-ray diffraction pattern for Gd sputtered Zirlo substrate sample.

X-ray diffraction signals typically come from the top few microns of the surface, and as a result the signal from the gadolinium is attenuated in relation to the strong signal from the underlying zirconium alloy substrate. There is no evidence of any oxidation during the sputtering process and a comparison with the observed Gd peak intensities with those of Gd in JCPDS files indicates that some texturing (preferential film growth along certain planes) may have occurred. Similar trends were observed for the Zircaloy-4 samples.

Characterization Ion Beam Surface Treatment (IBEST) of Gd-sputter deposited samples

The Gd sputtered samples were subjected to the IBEST treatment at Sandia National Laboratories using high energy (600 keV) Ne⁺ ions. A schematic illustration of the IBEST process is shown in Figure 7.

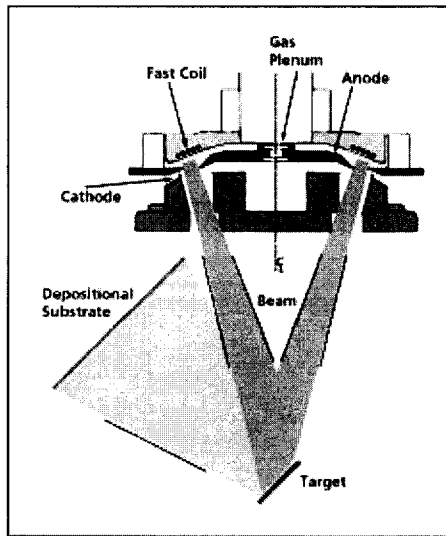


Figure 7. Illustration of the IBEST process at Sandia National Laboratories that is being used for surface alloying of Gd and Zr-alloy substrates.

X-ray diffraction pattern for the Zirlo sample that was deposited with a $0.5\mu\text{m}$ Gd film and then IBEST treated is shown in Figure 8. No significant peaks of Gd were observed, however this is not unexpected since conventional x-ray diffraction used in this study includes substantial substrate effects. In light of this it should be noted that due to ablation effects, the thickness of the Gd containing surface layer is probably much lower than $0.5\mu\text{m}$. Consistent with this explanation, as will be shown later, significant Gd peaks were observed when a $1\mu\text{m}$ film of Gd was sputter deposited and IBEST treated.

Scanning electron microscopy with EDS (Energy Dispersive Spectroscopy) chemical analysis capabilities was performed on the IBEST treated samples. High magnification examination of the Zirlo sample showed a uniform featureless structure with no evidence of phase separation. EDS analysis of the alloy however showed the presence of Gd on the surface. The results of these SEM evaluations are shown in Figure 9.

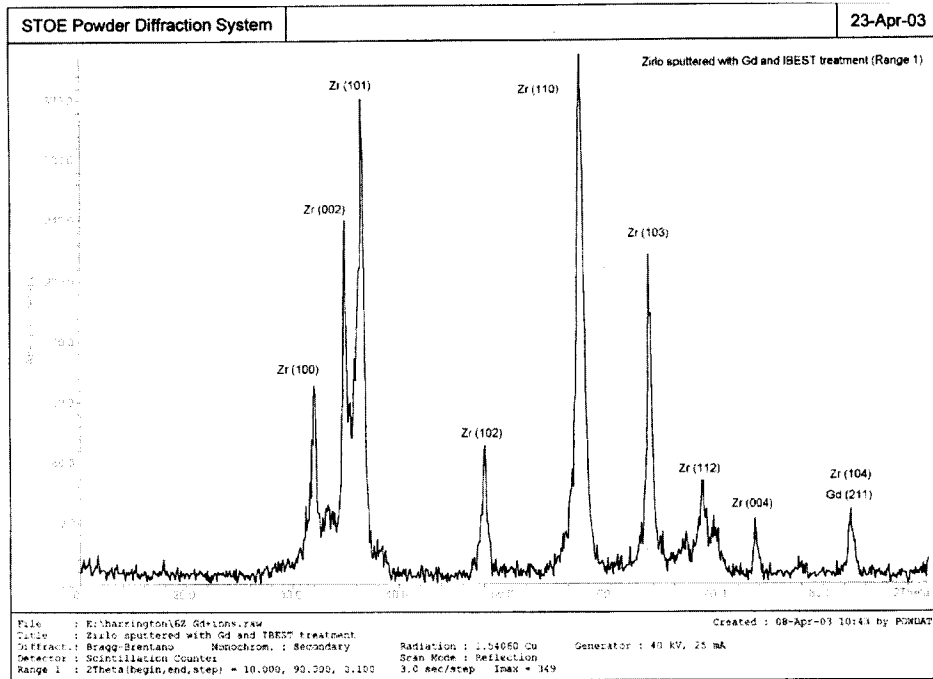


Figure 8. X-ray diffraction pattern of the Zirlo sample that was deposited with a 0.5 μm of Gd and then IBEST treated.

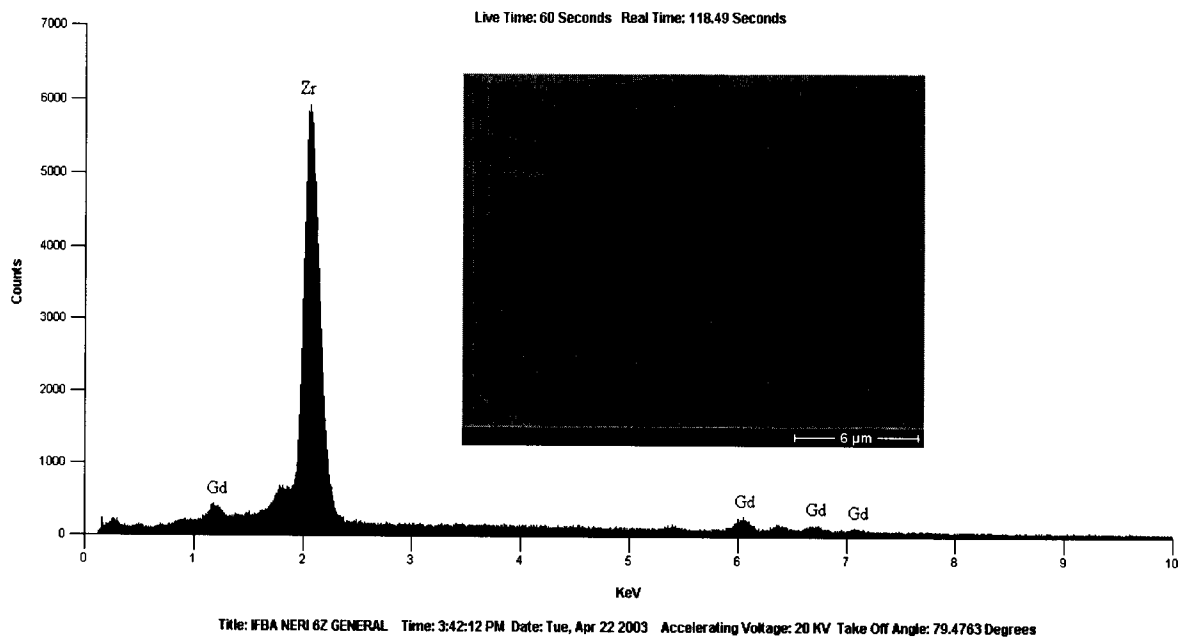


Figure 9. Scanning Electron Microscopy Energy Dispersive Spectroscopy (SEM-EDS) analysis showing the presence of Gd in the near-surface regions of the Zr-alloy. Gd signals are attenuated because of the electron penetration depth exceeds the alloyed layer depth. High magnification imaging shows a homogeneous structure devoid of phase separation.

Figure 10 shows the results of near-surface chemical analysis of the zirconium alloy after gadolinium surface alloying as determined by Rutherford Backscattering Spectroscopy (RBS). The results show that substantial amount of gadolinium co-exists in the near-surface regions of the sample along with the substrate material Zr.

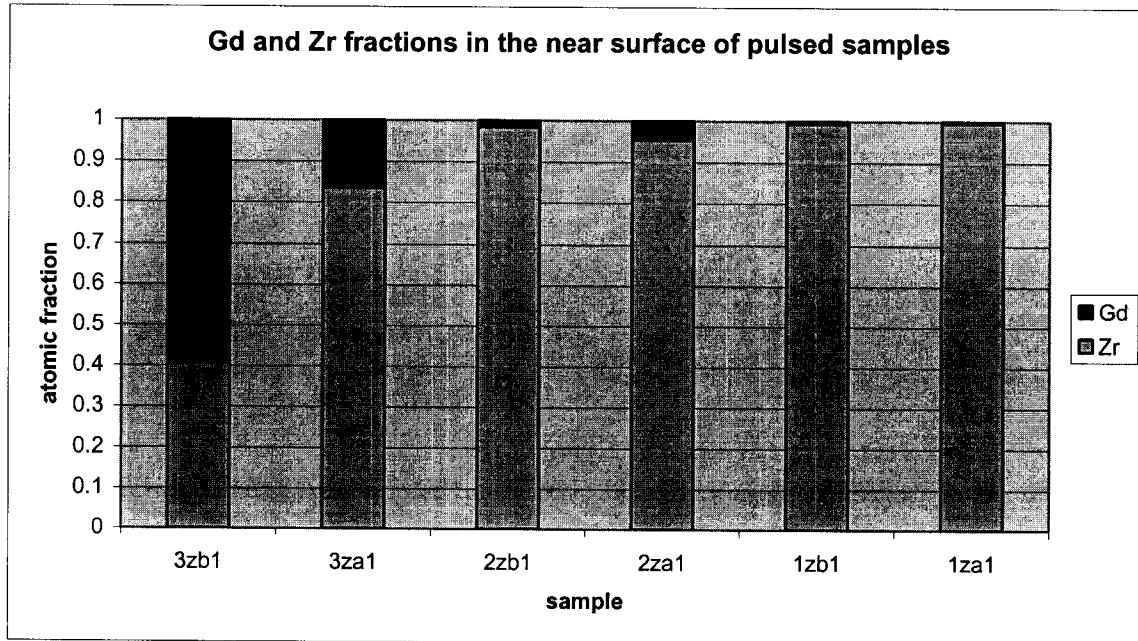


Figure 10: Rutherford Backscattering Spectroscopy (RBS) results showing the co-existence of gadolinium and zirconium in the near-surface regions of the material. Results are shown of samples that experienced different process conditions. Sample 3zb1 shows the best alloying between Gd and Zr.

Experiments with 1 μ m gadolinium sputtered film followed by IBEST showed a substantially increased incorporation of Gd into the zirconium alloys. Figure 11 shows the x-ray diffraction patterns for this sample. These observations appear to indicate that a 1 μ m Gd film would be more desirable for this application than a 0.5 μ m film of Gd, from the standpoint of incorporating greater amounts of IFBA in the cladding material. No intermetallics of Gd and Zr are observed indicating that Gd might be present largely as a solid solution. This observation is supported by transmission electron microscopy of the 1 μ m gadolinium film deposited and IBEST treated sample shown in Figure 12 where a homogeneous structure with no phase separation is observed.

These observations and results are significant because they demonstrate that despite the negligible mutual solubility between Gd and Zr, they can be homogeneously alloyed using non-equilibrium ion bombardment and rapid solidification approaches.

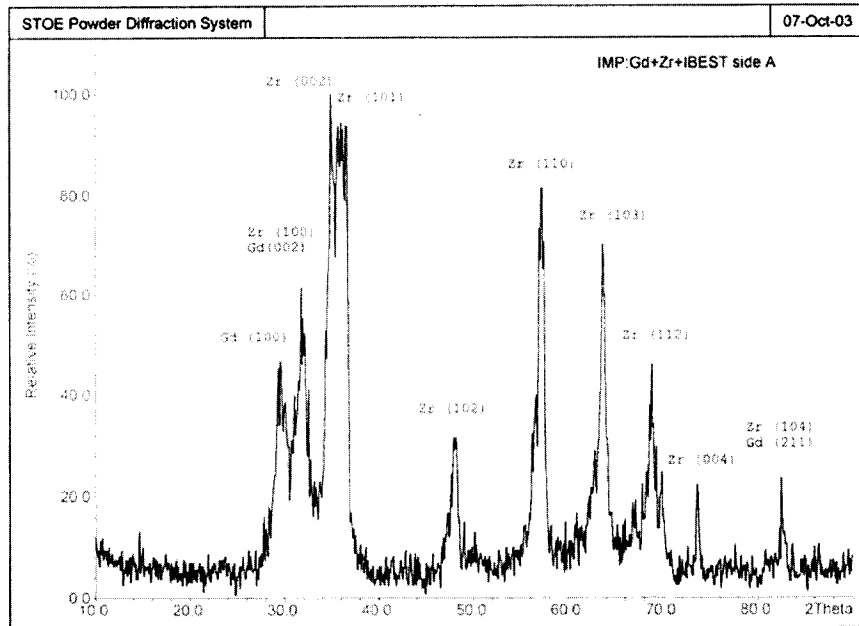


Figure 11. X-ray diffraction pattern of a Zr-alloy after 1 μ m thick Gd sputter deposited film followed by IBEST. A comparison of this with a 0.5 μ m Gd film (Figure 8) shows a substantially larger amount of Gd-alloying in this case.

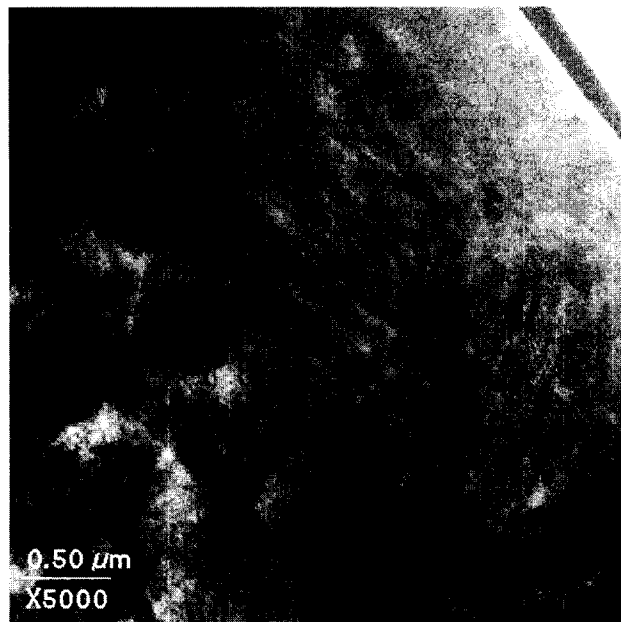


Figure 12. Transmission Electron Microscopy image of the Gd-incorporated Zr-alloy. The taper in the top right side is the sample surface. The structure is homogeneous and there is no evidence of phase separation. Samples were prepared by Focus Ion Beam (FIB) technique.

Results of low-load microhardness testing performed across the entire thickness of the two zirconium alloys before and after IBEST treatment is shown in Figure 13. No drastic change in microhardness trends are observed before and after IBEST treatment indicating that there was no significant degradation of base material microstructure due to the heat flux from the IBEST treatment.

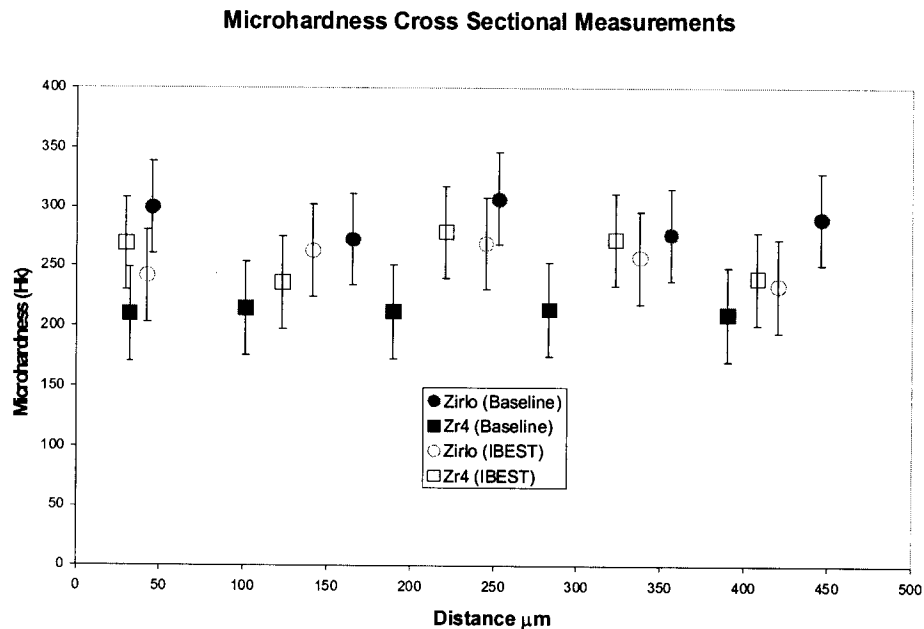
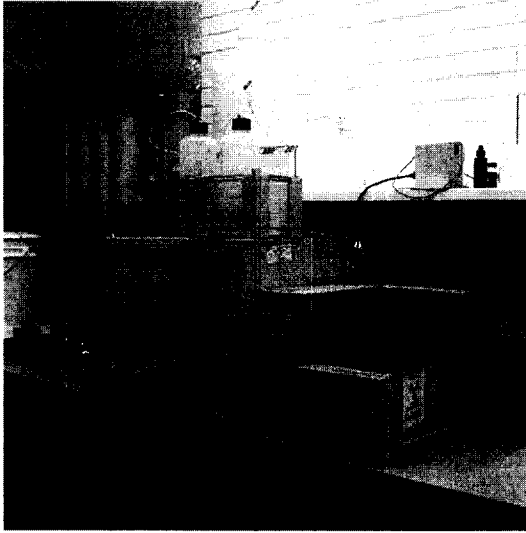


Figure 13. Low-load microhardness tests across the thickness of the Zirlo and Zr-4 samples before and after the IBEST treatment. No significant changes in hardness profile was observed indicating that there was no major degradation in the bulk microstructure as a result of the heat flux during the IBEST treatment.

Autoclave testing and post-autoclave testing analysis: Autoclave testing of the Gd-alloyed samples were performed in the autoclave facilities at Westinghouse at 800F and 100 atmospheres pressure in a steam environment. Figure 14 shows the automated autoclave test facilities at Westinghouse where the samples were tested. Our initial autoclave testing results have shown that oxide scaling began to occur on the sample surface when tested in 800F steam for one day. Figure 15 shows the surface of the zirconium alloy control sample and gadolinium-alloyed sample after autoclave testing for 1 day, showing severe oxidation of the gadolinium alloyed sample. Figure 16 shows a high magnification SEM image of the oxide formation and scaling. SEM-EDS analysis indicated that some samples showed predominantly gadolinium-oxide (Figure 17) whereas in others there was no significant Gd (Figure 18).

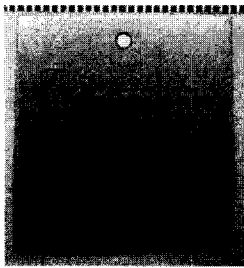


(a)

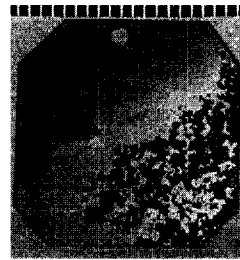


(b)

Figure 14. (a) Automated autoclave test facilities (at Westinghouse where the samples were tested at 800F/100 atmospheres in a steam environment and (b) specimen rack for suspending samples in the autoclave.



(a)



(b)

Figure 15. Surface of (a) control zirconium alloy sample and (b) gadolinium-alloyed sample (right) after autoclave testing for one day at 800F in pressurized steam environment.

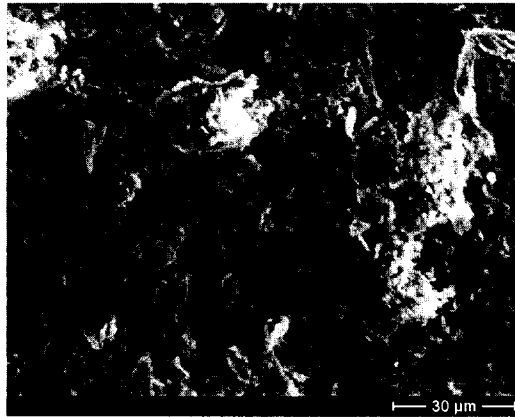


Figure 16. SEM photomicrograph showing surface oxidation and scaling after autoclave testing.

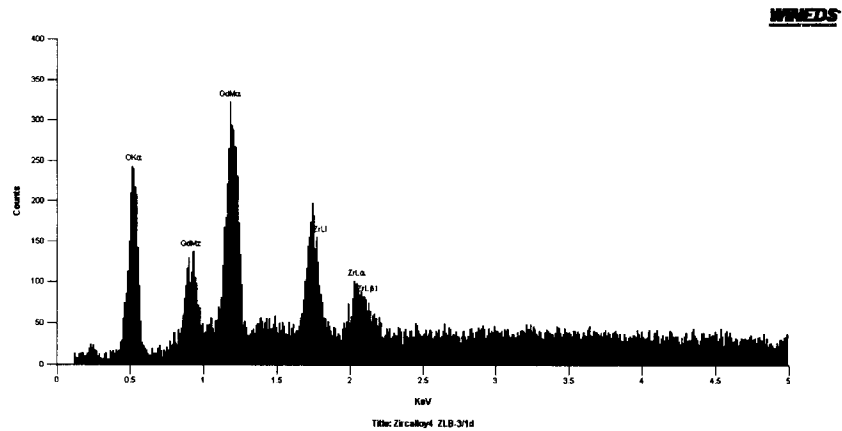


Figure 17. SEM-EDS analysis of the samples that developed an oxide scale (after autoclave testing) consisting predominantly of gadolinium oxide..

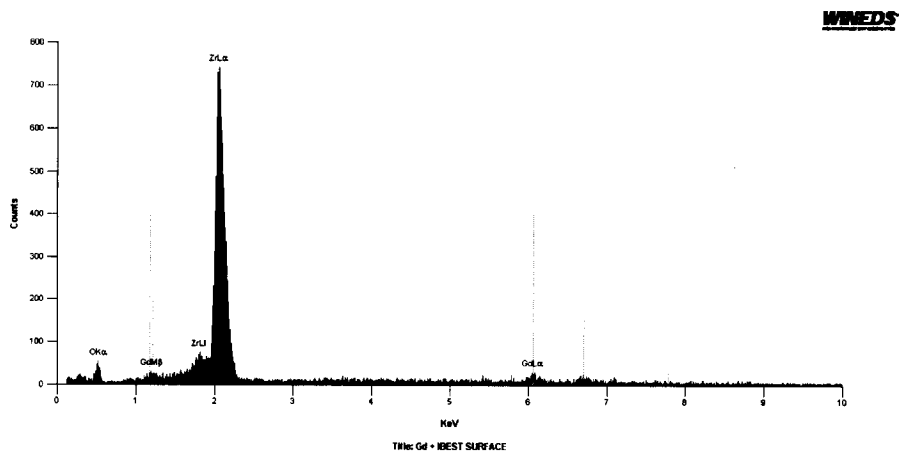


Figure 18. SEM-EDS analysis of the samples that developed an oxide scale (after autoclave testing) but showed regions were devoid of Gd.

An understanding of the oxidation and spalling characteristics of the gadolinium alloyed samples can be achieved to some extent by examining some of the relevant properties of the oxides of gadolinium and zirconium listed in Table 1.

Table 1: Specific properties of gadolinium and zirconium oxides pertinent to oxide forming and scaling.

<p>Oxide heat of formation: Gd₂O₃: -1820 KJ/mole ZrO₂: -1100 KJ/mole Pilling-Bedworth ratio, R= V metal oxide/Vmetal R=1.55 for ZrO₂ on Zr R= 1.7 for Gd₂O₃ on Gd R=2.95 for Gd₂O₃ on Zr High R values promote spalling</p>

It may be noted that gadolinium has an extremely high negative heat of formation, which is indicative of its strong propensity for oxide formation. The high Pilling-Bedworth ratio for this oxide with respect to zirconium is indicative of its propensity for spalling.

D. STUDIES OF BORON SURFACE ALLOYING

Studies on surface alloying were performed using a methodology similar to the gadolinium work reported earlier. As in the case of gadolinium, boron was successfully incorporated into the zirconium alloys using a sequence of sputtering and IBEST processing. However, the more significant result here was the demonstration that autoclave testing did not significantly alter the corrosion resistance of zirconium-alloys. As mentioned in previous reports,

Experimental Approach:

In the IBEST processing system at Sandia National Laboratories, there is a dose gradient (as one moves away from the centerline) on the IBEST sample stage, which results in different levels of alloying, based on sample location. For the boron experiments, the presence of this dose gradient was utilized to provide valuable information regarding the effect of dose on surface boron/zirconium melting. One side of five samples each of Zirlo and Zircaloy-4 was sputter coated with 0.75 μ m film of boron. One sample of each alloy was retained for analysis of the as-sputtered structure and the remaining four samples of each alloy were subjected to the IBEST process. Figure 1 shows the layout of the samples for the IBEST treatment. Since boron has a substantially higher heat of fusion compared to gadolinium, nitrogen ion species was used as the source of inputting heat for alloying rather than neon ions, which were used for the gadolinium experiments. All four Zircaloy-4 samples were retained between Sandia National Laboratories and University of Wisconsin for basic material characterization work, whereas the four samples of Zirlo were sent to Westinghouse for autoclave testing.

Materials characterization:

Examination of sample No. 1 (please refer to Figure 19 for sample numbers) of Zircaloy-4 at high magnification under a scanning electron microscope showed a single phase structure with a lath morphology (Figure 20). This type of structure has been observed in previous studies on IBEST treatment of Ti-alloys and is indicative of complete melting at the surface. SEM-EDS analysis of the surface showed the presence of boron, however boron being a light element is not accurately quantified by this technique. In contrast, sample No. 3 of Zircaloy-4 showed a crusty surface that is indicative of partially melted boron (Figure 21). As expected, SEM-EDS analysis of the surface of this sample

indicated nearly 100% boron. This effect can be directly related to the lower dose of nitrogen ions (less heat input) received by sample No. 3 as compared to sample No. 1.

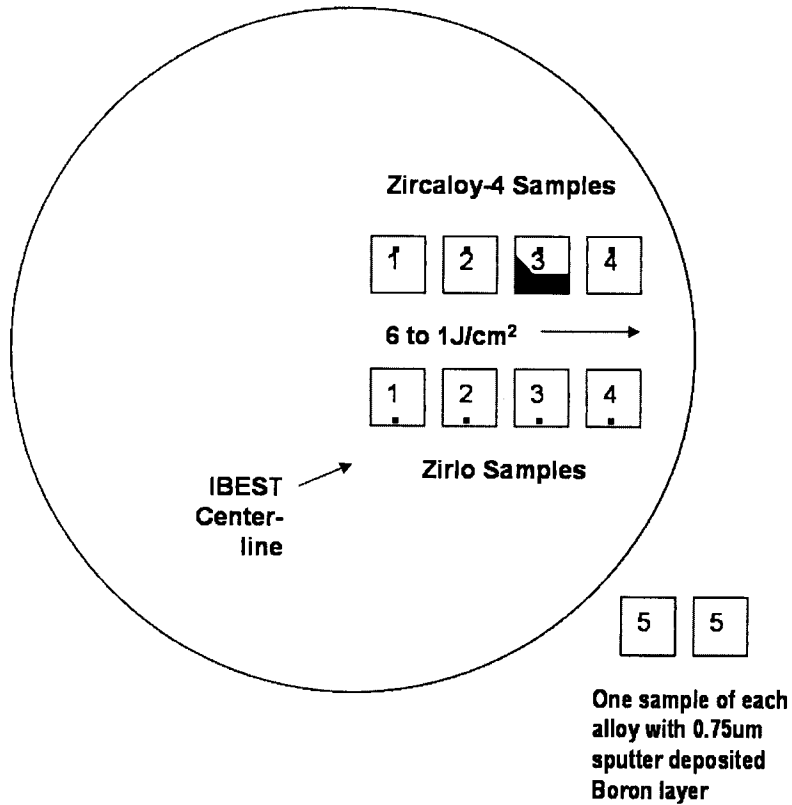


Figure 19: A schematic illustration of the sample arrangement on the IBEST system stage for alloying boron into zirconium alloys.

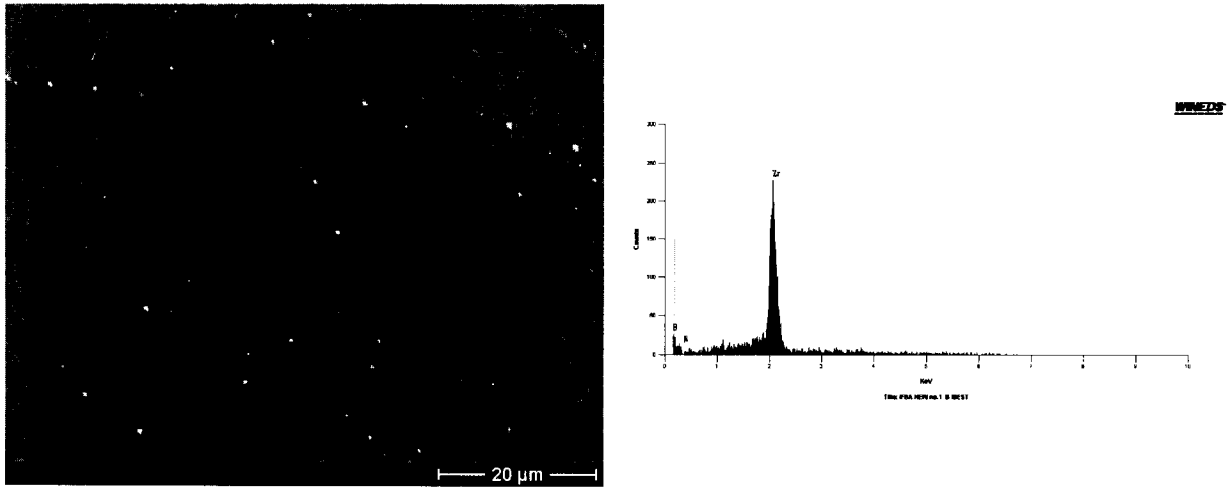


Figure 20. Scanning Electron Micrograph (left) of sample No. 1 of Zircaloy-4 showing a structure indicative of complete melting of boron and resolidification of boron-zirconium alloy. Corresponding EDS analysis (right) showed the presence of boron (green line), however boron being a light element is not amenable to exact quantification by EDS analysis.

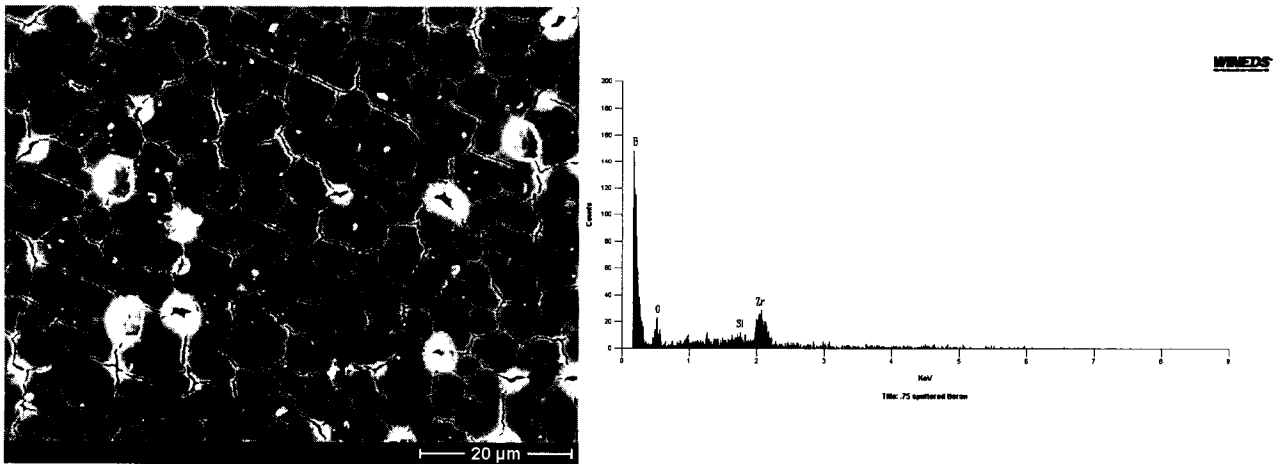


Figure 21: Scanning Electron Micrograph (left) of sample No. 3 of Zircaloy-4 showing a structure indicative of partially melted of boron. Light spots on the surface are zirconium alloy droplets splattered from the other half of the sample. As expected, the corresponding EDS (right) showed the presence of nearly 100% boron.

Auger analysis, which provides an accurate estimate of boron content, was performed on sample No. 1. The results, shown in Figure 22 indicate a complete co-existence of boron and zirconium. Throughout the sputtered depth the boron concentration was uniform at about 25 at%. Figure 23 shows the laser surface profilometry of the Auger analysis sputter crater. Even after sputtering for a period in excess of 300 minutes, the boron concentration maintained a steady concentration of about 25 atomic%. The depth of the sputter crater was measured at $3.75\mu\text{m}$ and it is estimated that the boron was incorporated to depths of 4 to $5\mu\text{m}$. SEM cross-sectional examination (Figure 24) of the boron alloyed samples confirm this observation. A diffusion layer of boron-alloyed material is clearly seen after etching the sample. Ripples representing flow of liquid “frozen-in” are a testament to the ultra-high quench rates experienced by the thin skin of molten material in the IBEST process. In addition, no evidence of the bombarding species nitrogen was observed, which would have been undesirable because of the hard, brittle nature of the compound, ZrN. We believe that these are significant results in terms of the overall goals of this NERI project.

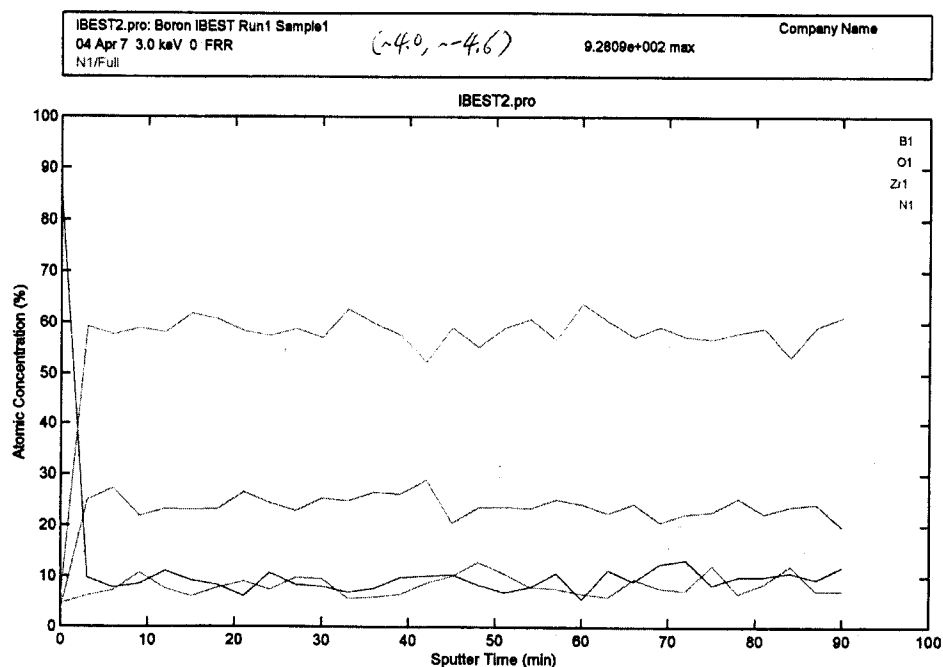


Figure 22: Auger composition vs depth (sputter time) analysis showed uniform coexistence of boron and zirconium (at about 25 at.% boron).

From a basic materials science standpoint, the following points are worthy of attention. Thermodynamically, the phase most favored to form in this case is the compound, ZrB_2 . This compound however contains 66 at.% boron, whereas the Auger analysis in Figure 22 shows only 25 at% boron. This precludes the possibility that a uniform layer of ZrB_2 formed on the surface. The other possibility, although less favorable in the thermodynamic/kinetic hierarchy, is the formation of a fine particle distribution of ZrB_2 in the Zr-alloy matrix. Since Auger analysis detects species in their elemental form, a profile as shown in Figure 22 could potentially result from the presence of such a fine particle distribution of ZrB_2 . However, this possibility can be precluded with a high degree of certainty for the following reasons: (i) high magnification SEM showed a single phase and no second phase particles were observed, (ii) x-ray diffraction did not show any ZrB_2 peaks, and (iii) low-load (10 gram) microhardness testing (Figure 25) showed only a minor increase in hardness, which would not be the case if ZrB_2 had formed. The marginal increase in microhardness appears to be typical of solid solution strengthening which refers to an increase in hardness of a metal when alloying elements are dissolved in its lattice structure. An examination of the Zr-B phase diagram indicates negligible solubility of boron in zirconium. The significantly enhanced solubility observed in this case could stem from the very high solidification rates typical of the IBEST process, that are known to result in the "solute-trapping" effect which leads to an extension in solute (boron) solubility.

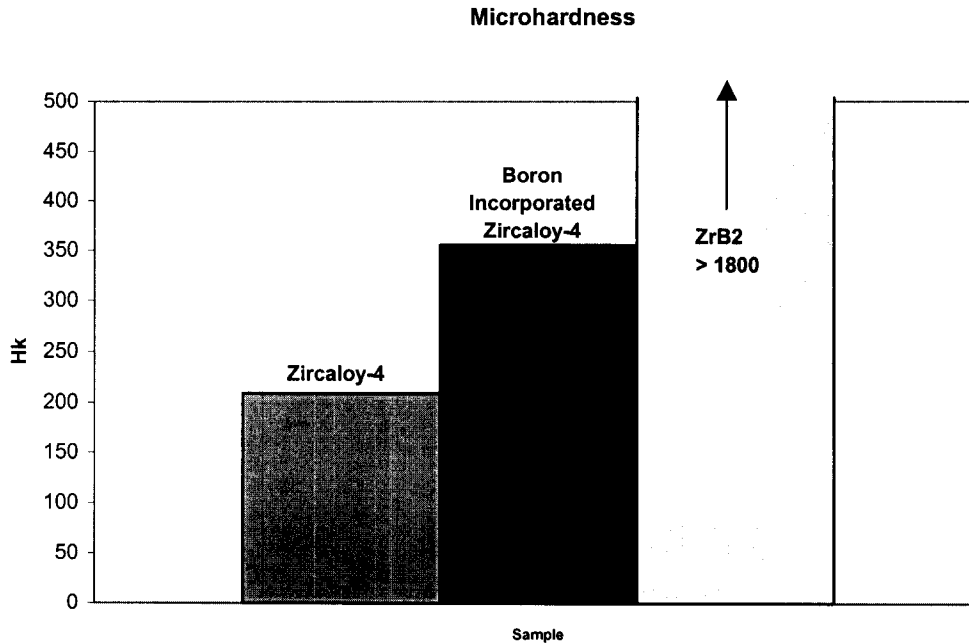


Figure 25: Low-load (10 gram) microhardness testing showing the hardness of Zircaloy-4, boron-alloyed Zircaloy-4 (sample No. 1) and the theoretical hardness of ZrB₂. This result suggests that boron is most-likely present as a solid solution in the Zircaloy-4.

Autoclave Testing:

Autoclave testing of the boron-alloyed samples was performed at Westinghouse. The tests were conducted at 800F for 3 days, with weight gain and surface examination being made daily. Examination of the surface of the samples showed no visible signs of corrosion (Figure 26). The samples, for the most part, appeared similar to the control, untreated Zirlo samples that were placed alongside in the autoclave. Figure 27 shows the weight gain measurements made of the boron-alloyed samples as function of the position of the samples on the IBEST stage. For comparison, the weight gain (per unit area) of the Zirlo control samples tested under similar conditions is also shown. All boron-alloyed samples performed reasonably well, however sample No. 1 performed the best and showed a weight gain almost identical to the control Zirlo sample. This is consistent with the observation made for the untested boron-alloyed samples of Zircaloy-4, where the sample in position No. 1 exhibited the best alloying. Figure 28 shows the

SEM micrograph and EDS analysis of boron-alloyed Zirlo (Sample No. 1) after autoclave testing. No significant oxidation in the form of particulates or any evidence of phase separation was observed. EDS analysis showed the presence of boron on the surface. Lack of oxidation or second phase separation and the continued presence of boron after autoclave testing are other significant results in terms of the overall objectives of this NERI project. Figure 28 also shows the surface of an as-received Zirlo sample after autoclave testing under similar conditions. Given that this control sample was not polished and had surface roughness, it is a reasonable conclusion that the corrosion resistance of the alloy was not diminished after boron alloying surface treatment. Further evidence of this is borne out by cross-sectional examination of the boron IBEST-treated samples and the control samples after autoclave testing which shows a similar build-up of the oxide corrosion product in both cases (Figure 29).

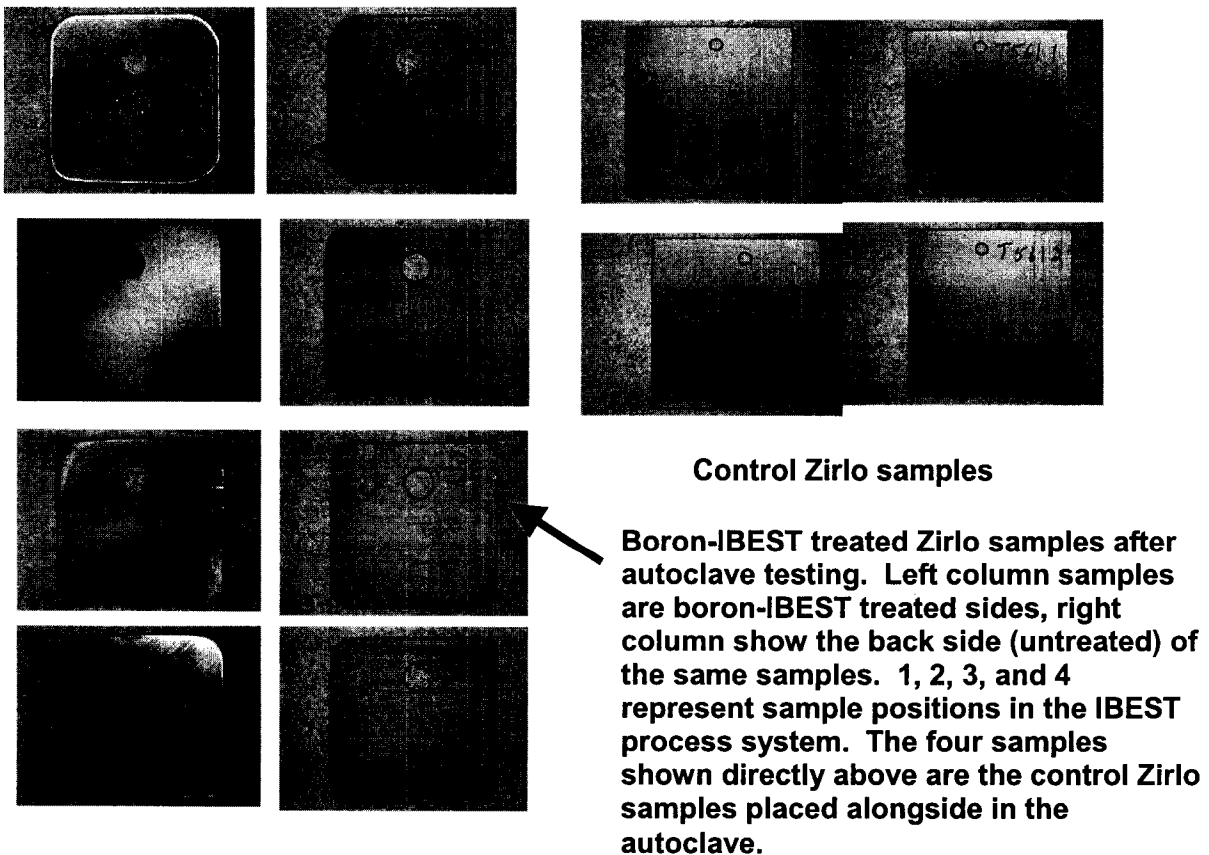


Figure 26: Surface of various samples after autoclave testing at 800F for 3 days.

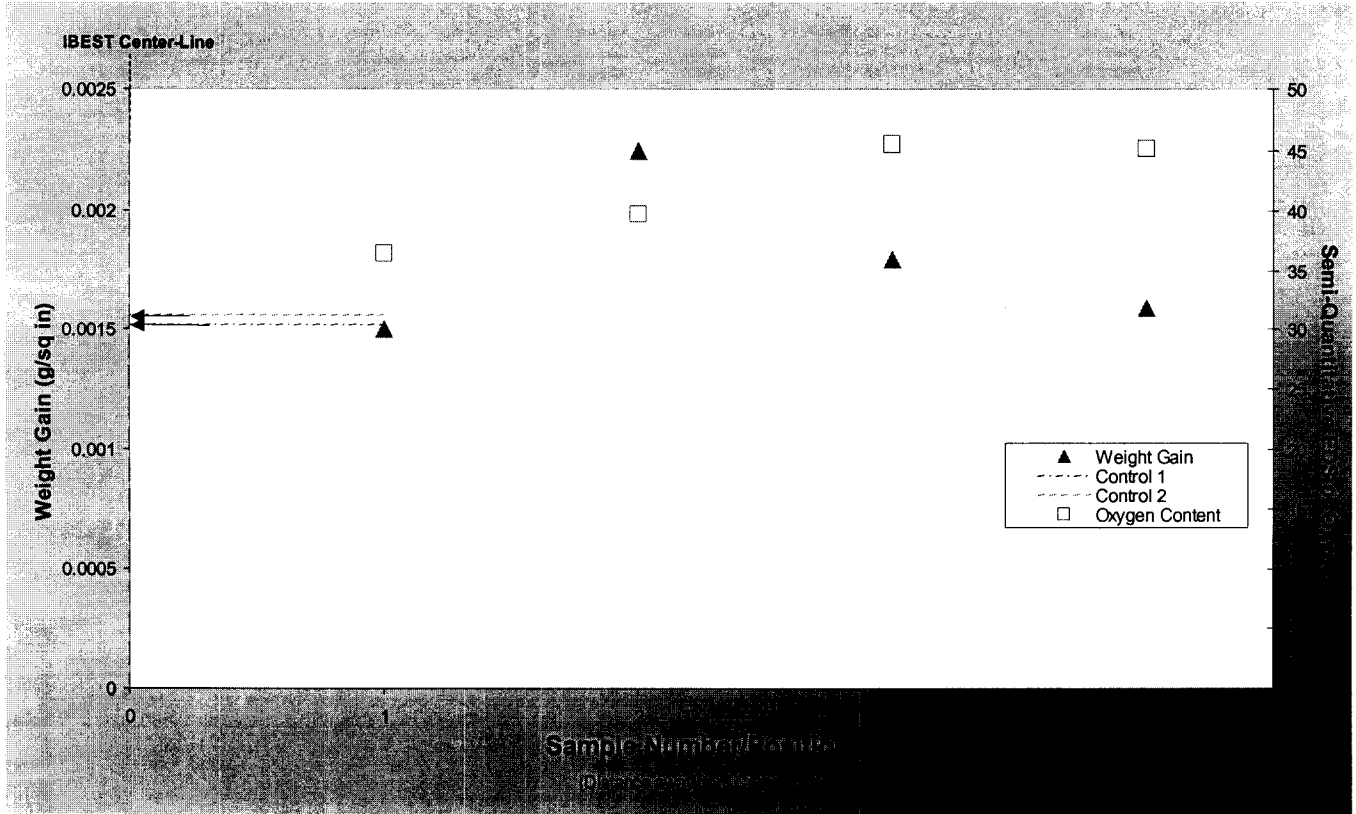
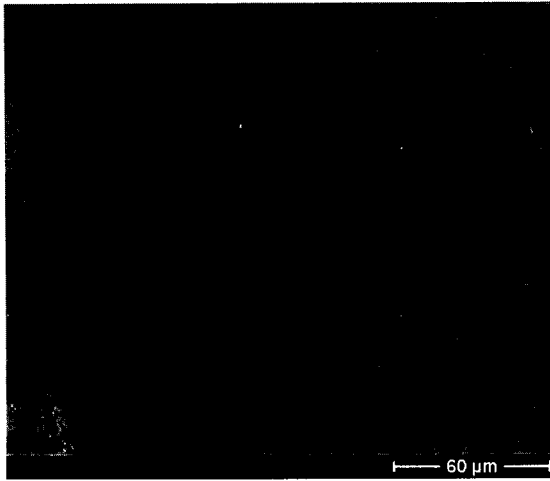
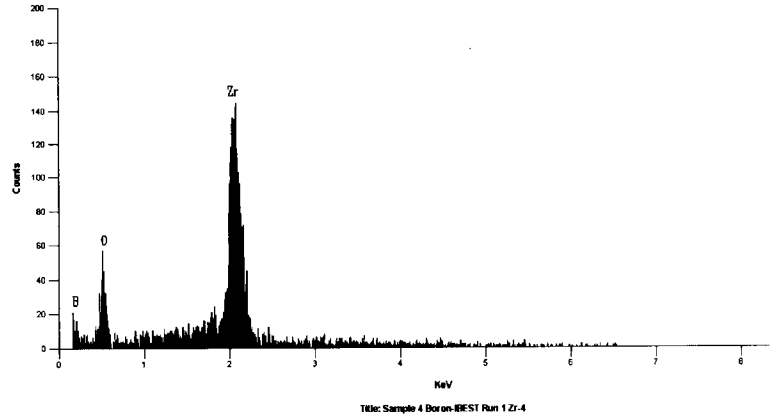


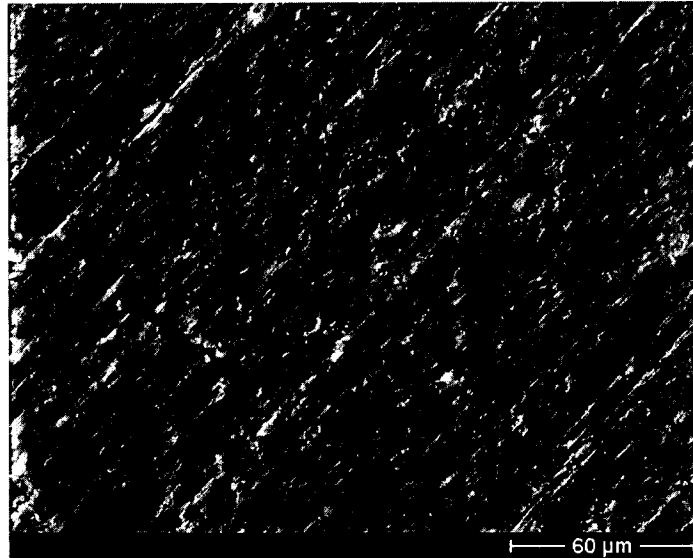
Figure 27: Weight gain of boron-IBEST treated Zirlo samples after steam autoclave testing for 3days at 800F, as function of the sample position on the IBEST stage. For comparison, the weight gain for the untreated, control Zirlo samples are also shown. Approximate oxygen content of the surface of samples is also indicated.



(a)



(b)



(c)

Figure 28: (a) Scanning electron micrograph (left) of the surface of the boron-IBEST treated Zirlo sample (No. 1) after autoclave testing at 800F for 3 days, showing no oxide particulates or second phase precipitation, (b) EDS analysis of the surface showed that boron is still present, however as expected the oxygen content is higher compared to the untested sample, (c) control Zirlo sample that was autoclave tested under similar conditions.

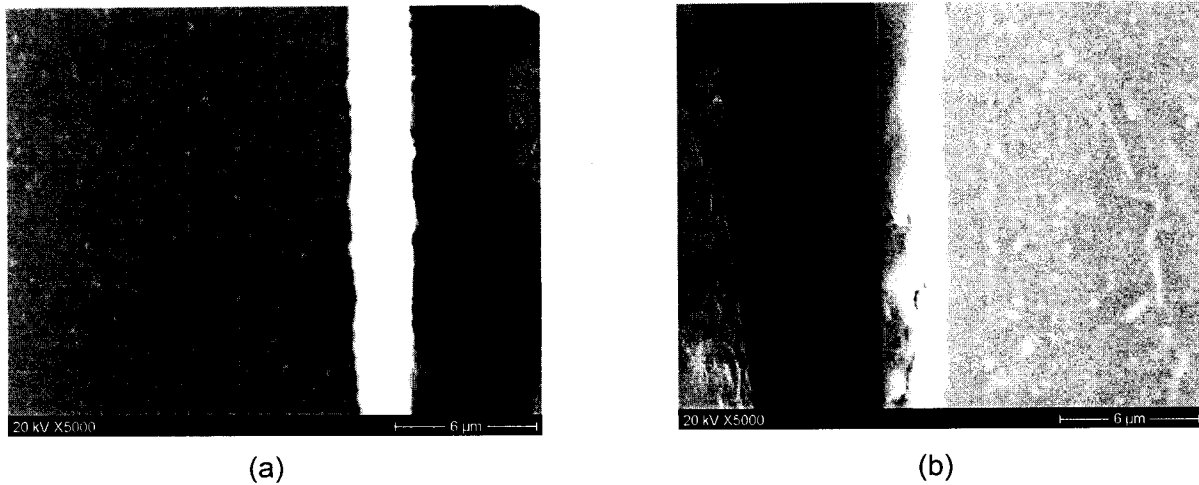


Figure 29. Cross-sectional SEM micrograph showing a nearly identical build-up of the oxide corrosion product after autoclave testing for (a) control sample and (b) boron-IBEST treated sample.

Numerical simulations for 1 μm boron film thickness:

Based on commercial requirement about 2mg of B10 per inch of tube length and clad geometry, it was calculated that a boron sputter layer in excess of 1 μm thickness would be required. As a result, the next experiments were performed by sputter depositing a 1 μm boron film thickness followed by the IBEST process.

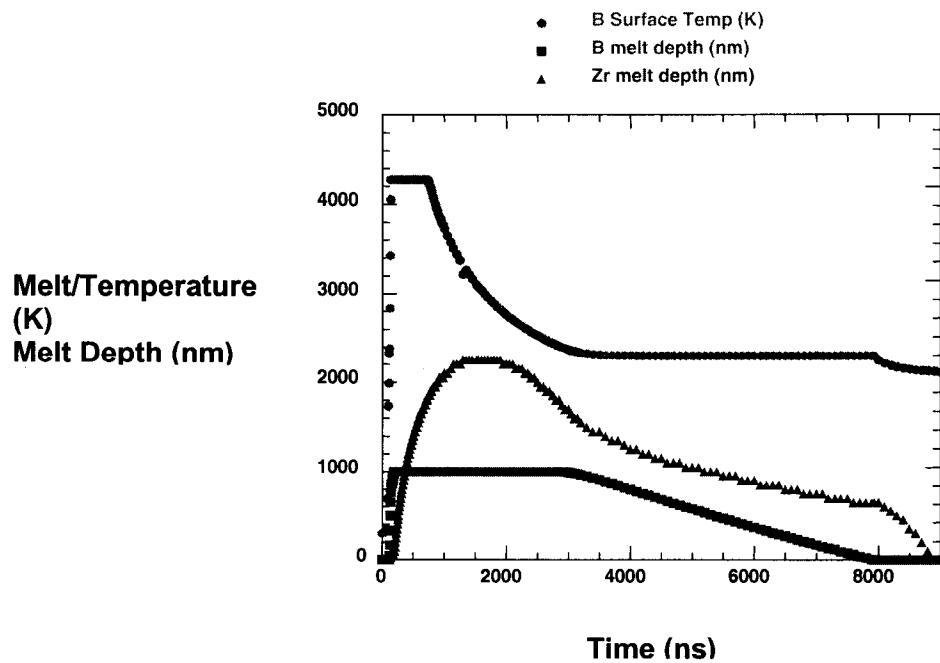


Figure 30. Numerical simulation of melting, liquid diffusion, and rapid solidification for a 1 μm boron film sputter deposited on Zr. The simulation uses an ion-materials interaction SRIM code and a liquid melting/diffusion code.

Figure 30 shows a numerical simulation of melt thickness and duration for a 1 μm boron film on zirconium alloy after IBEST bombardment with 6kJ/cm² nitrogen beam. The simulation shows that the entire 1 μm boron film and 2 μm of underlying zirconium will melt and the melt duration will be approximately 4000 nanoseconds. In other words, the simulation indicates that it would be possible to alloy 1 μm boron film using a 6kJ/cm² nitrogen beam.

IBEST surface alloying with 1 μm boron film:

For these experiments the samples were clustered close to the center-line of the IBEST system stage in order to minimize any gradients in energy. In addition, samples were treated with two levels of pulse shots 20 shots and 35 shots, but for the same total energy. Figure 31 shows the samples after sputter deposition with 1 μm boron film and treatment with the IBEST process.



Figure 31: Samples sputter deposited with 1 μm boron film and IBEST treated (on the IBEST sample stage at Sandia).

Examination of the surface of the IBEST-treated samples showed for the most part a uniformly melted surface with lath type structural morphology (Figure 32a). This type of structure is frequently observed in rapidly cooled Ti-alloys and Zr-alloys. In some regions high magnification imaging showed sub-micron sized droplets splattered from the ion bombardment and melting process (Figure 32b). But for the most part the surface was indicative of uniform melting and alloying.

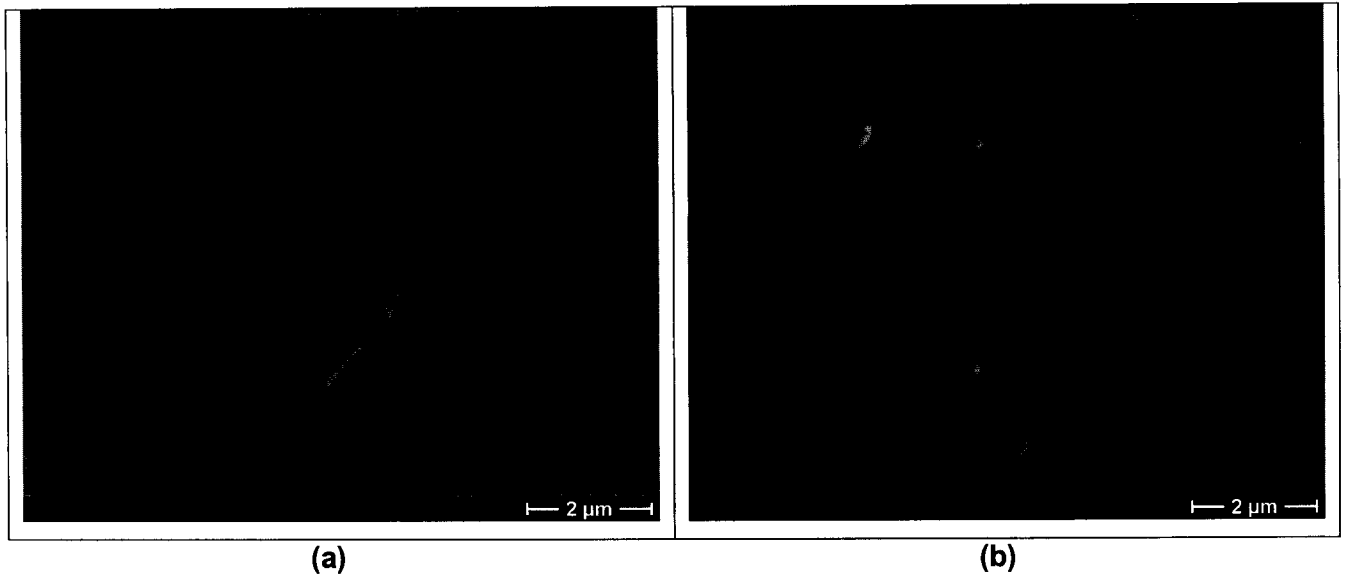


Figure 32. (a) High magnification SEM imaging of the surface of the 1 μ m boron IBEST treated sample showing uniform melting and surface alloying (b) fine sub-micron droplets from the energetic ion bombardment and melting were also observed.

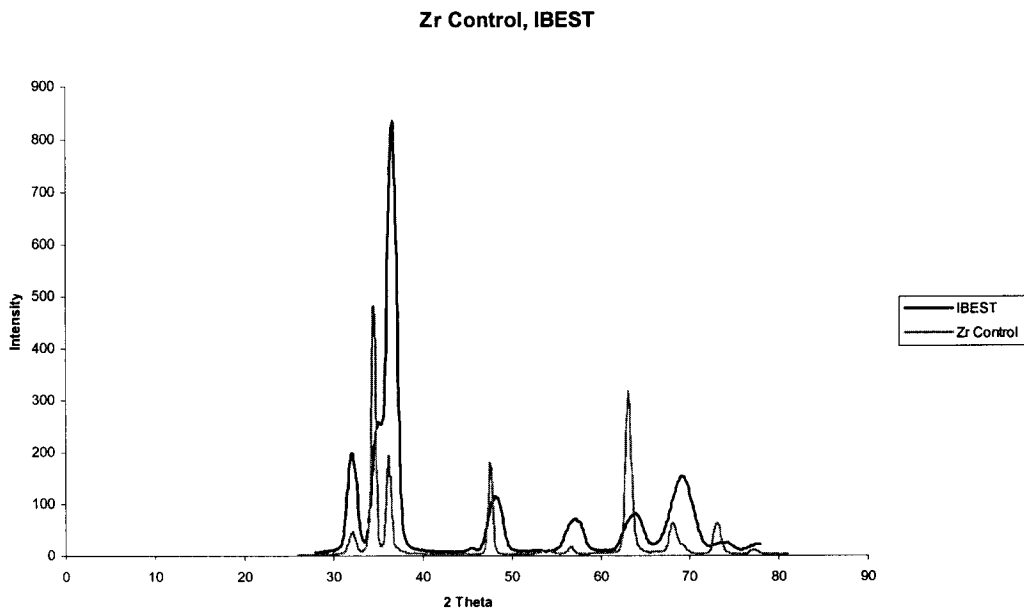


Figure 33. Grazing incidence x-ray diffraction for zirconium (control) and 1 μ m boron IBEST treated sample. Peak broadening for the IBEST sample is indicative of surface stresses caused by alloying.

Figure 33 shows the results of the grazing incidence x-ray diffraction performed on the control zirconium alloy and the 1 μm boron IBEST treated sample. Significant peak broadening is observed for the IBEST treated sample which is a manifestation of the surface stresses induced by the forced alloying of large quantities of boron into the zirconium alloy.

Figure 34 shows cross-sectional transmission electron microscopy images prepared using the Focused Ion Beam (FIB) technique. Fig. 34 shows the image of sputter deposited 1 μm boron (white band). Fig. 32b and c shows the images after surface alloying with IBEST. Fig. 34b is a boron map, where the white interspersed regions represent boron extending up to at least 2 μm below the surface. Fig. 34c shows the homogeneous solidification structure of the near-surface alloyed region.

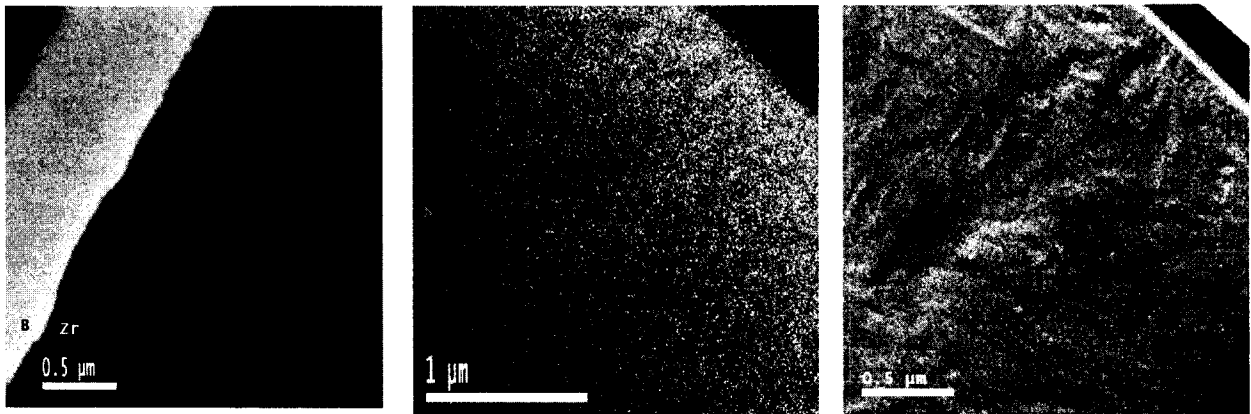


Figure 34. Cross-sectional transmission electron microscopy images prepared using the Focused Ion Beam (FIB) technique, (a) sputter deposited 1 μm boron (white band), (b) is a 'boron map' after IBEST treatment where boron is represented by the white regions, and (c) homogeneous solidification structure of the near-surface alloyed region after IBEST.

Autoclave testing:

Figure 35. shows the surface of the 1 μm boron IBEST treated sample after autoclave testing in a steam environment at 800F for 14 days. The plan view (a) of the surface shows marginal oxidation and the cross-sectional view shows a well-developed oxide layer comparable in thickness to the control zirconium alloy.

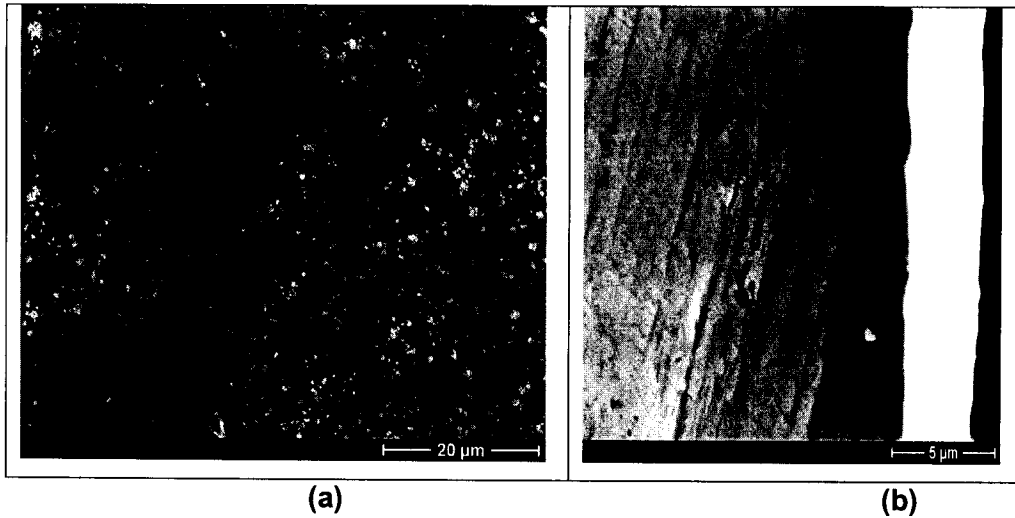


Figure 35. Oxidation on the surface of 1µm boron IBEST treated sample after autoclave testing for 14 days in a steam environment at 800F. Oxidation was comparable to the control zirconium alloy sample, (a) plan view showing oxide particulates and (b) cross-sectional view showing an oxide about 3µm thick.

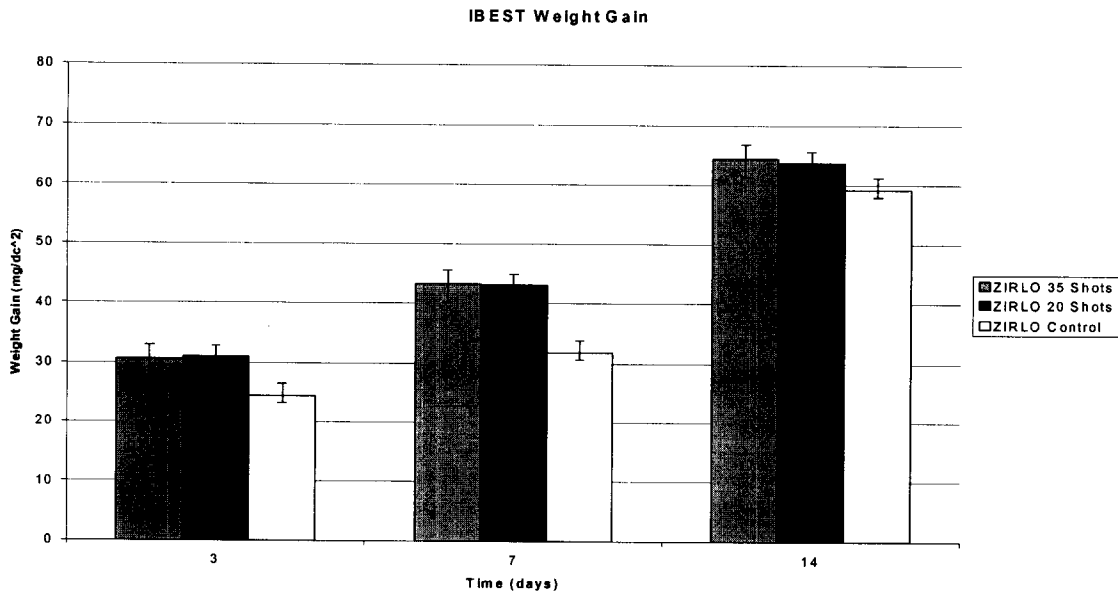


Figure 36. Weight gain due to the build-up of the oxide layer corrosion product on Zirlo and Zirlo that has been 1 µm IBEST treated sample with 20 and 35 pulse shots. Samples were exposed to 3, 7, and 14 days to steam at 800F. The important conclusion is that the IBEST processing does not alter the corrosion behavior of Zirlo in a significant manner.

Figure 36 shows the thickness of the oxide layer corrosion product for Zirlo and 1 μ m IBEST Zirlo sample treated with 20 and 35 pulse shots. The data is plotted based on exposure times of 3, 7, and 14 days. There is no significant difference in oxidation performance between samples that were IBEST treated with 20 and 35 shots and the IBEST treatment only marginally affects (to the detriment) of the already excellent corrosion resistance of Zirlo.

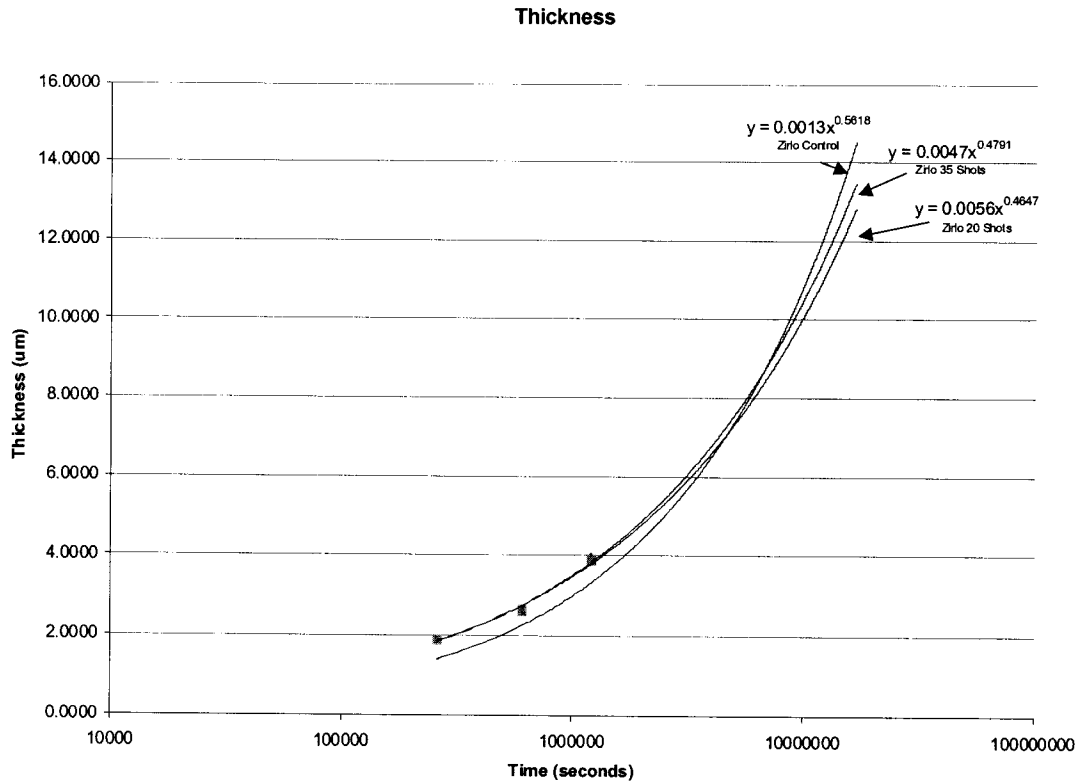


Figure 37. Growth of the oxide layer corrosion product on Zirlo 1 μ m IBEST Zirlo sample treated with 20 and 35 pulse shots. Samples were exposed for 3, 7, and 14 days to steam at 800F.

Based on this limited data, the thickness of the oxide film was related to the exposure time, as follows:

For control Zirlo sample:

$$\text{Thickness (mm)} = 0.0013(\text{Exposure Time in seconds})^{0.5618}$$

For 1 μ m IBEST Zirlo sample treated with 20 pulse shots:

$$\text{Thickness (}\mu\text{m)} = 0.0056(\text{Exposure Time in seconds})^{0.4647}$$

For 1 μ m IBEST Zirlo sample treated with 35 pulse shots:

$$\text{Thickness } (\mu\text{m}) = 0.0047(\text{Exposure Time in seconds})^{0.4791}$$

Figure 37 also shows the extrapolated values for 6 months exposure assuming (for the sake of argument) that this is the period of initial reactivity. These values should be deemed to be approximate, however the most significant conclusion from this study is that the corrosion resistance of the Zirlo is not significantly affected by the boron IBEST surface treatment.

Weight gain measurements for Zirlo and Zircaloy-4 samples with and without 1 μm boron IBEST surface treatment, after exposure to supercritical water at 800F for 3 days showed that for Zirlo the number of pulse shots (20 and 35 pulse shots) did not have an influence on corrosion performance. For Zircaloy-4 however the decrease in corrosion resistance due to the IBEST treatment was a bit more pronounced, but still within the limits of acceptance. For Zircaloy-4, the 20 pulse shot samples performed slightly better than the 35 pulse shot samples.